ChemPubSoc Europe

DOI: 10.1002/cplu.201600222

CHEMPLUSCHEM Full Papers

Syntheses and Optical Properties of Azo-Functionalized Ruthenium Alkynyl Complexes**

Dilan Wei,[a] Mahesh S. Kodikara,[b] Mahbod Morshedi,[b] Graeme J. Moxey,[b] Huan Wang,[a] Genmiao Wang,[b] Cristóbal Quintana,[b] Chi Zhang,[a] Rob Stranger,[b] Marie P. Cifuentes,[a, b] and Mark G. Humphrey*[a, b]

The syntheses of *trans*-[Ru(C≡C-1-C_6H_4-4-N=N-1-C_6H_4-4-C≡C-1-C_6H_4-4-NO_2)Cl(L_2)$_2$] (L_2 = dppm (**Ru1**), dppe) (**Ru2**)), *trans*-[Ru(C≡C-1-C_6H_4-4-N=N-1-C_6H_4-4-(*E*)-CH=CH-1-C_6H_4-4-NO_2)Cl(dppe)$_2$] (**Ru3**), and *trans*-[Ru(C≡C-1-C_6H_4-4-(*E*)-CH=CH-1-C_6H_2-2,6-Et_2-4-N=N-1-C_6H_4-4-NO_2)Cl(dppe)$_2$] (**Ru4**) are reported, together with those of precursor alkynes. Their electrochemical properties were assessed by cyclic voltammetry (CV), linear optical and quadratic nonlinear optical (NLO) properties assayed by UV/Vis-NIR spectroscopy and hyper-Rayleigh scattering studies at 1064 nm, respectively, and their linear optical properties in the formally Ru^{III} state examined by UV/Vis-NIR spectroelectrochemistry. These data were compared to those of analogues with *E*-ene and yne linkages in place of the azo groups. Computational studies using time-dependent density functional theory were undertaken on model compounds (**Ru2′**–**Ru4′**) to rationalize the optical behaviour of the experimental complexes.

Introduction

Materials that can modify the propagation characteristics of light (e.g. frequency, phase, path, etc) are urgently needed for applications in current and prospective photonics technologies. Organic molecules possessing such "nonlinear optical" (NLO) properties that can fulfill these desired functions generally contain π-systems with highly delocalizable electron density. Very early in the search for NLO-efficient organic molecules, it was found that dipolar species such as *p*-nitroaniline (PNA) and 4-dimethylamino-4′-nitrostilbene (DANS) were particularly active, although subsequent research with molecules possessing other multipolar charge distributions (quadrupolar, octupolar) has also afforded NLO-efficient materials.[1] Improvements to the classical donor–π-bridge–acceptor composition of molecules such as PNA and DANS have focussed on modifying all three components. Thus, the donor group strength increases on proceeding from amino and dimethylamino to julolidinyl and diphenylamino, and the acceptor group strength increases on proceeding from nitro to tricyanovinyl and 2-dicyanomethylen-3-cyano-4,5,5-trimethyl-2,5-dihydrofuran, while delocalization through the π-bridge is improved on proceeding from phenyl to heterocyclic moieties with a lower aromatic stabilization energy; all of these modifications favourably impact on NLO parameters. In other studies relating structure to NLO properties, it was noted that the key quadratic NLO coefficient β is increased on certain modifications of the phenyl-based π-bridge (proceeding from biphenyl to *Z*-stilbene, tolane, and *E*-stilbene, because biphenyl exhibits unfavourable *ortho*-H steric pressure, reducing bridge coplanarity, while compounds with a *Z*-stilbene bridge have decreased charge separation in the key excited state compared to that of *E*-stilbene analogues).[2]

In contrast to the aforementioned structural modifications that improve NLO performance, the incorporation of more electronegative heteroatoms such as nitrogen into the π-bridge in organic NLO materials (proceeding from *E*-ene- to imino- or azo-linked compounds) frequently leads to a reduction in β value due to charge localization at the electronegative nitrogen atom(s).[3] Nevertheless, the azo-linked compounds, in particular, are of interest as archetypical examples of photochemical switches; irradiation of azobenzenes at specific wavelengths can provide a facile means to reversibly convert between the *E*- and *Z*-configured forms, although thermal conversion of the *Z* form to the *E* form imposes constraints on the utility of this specific molecular switch.[4]

Replacing the organic donor group in the classical donor–π-bridge–acceptor molecular composition with a ligated metal unit can confer certain advantages: the flexibility of metal, valence electron count, coligands, and coordination geometry can all impact favourably on the molecular NLO coefficients,[5] while the facile reversible oxidation/reduction undergone by many metal complexes can introduce important functionality and the potential to function as molecular NLO switches.[6] We have previously reported that azo-containing arylalkynyl com-

[a] D. Wei, H. Wang, Prof. C. Zhang, Prof. M. P. Cifuentes, Prof. M. G. Humphrey
School of Chemical and Material Engineering, Jiangnan University
Wuxi, Jiangsu Province 214122 (P. R. China)
E-mail: mark.humphrey@jiangnan.edu.cn

[b] M. S. Kodikara, Dr. M. Morshedi, Dr. G. J. Moxey, Dr. G. Wang, C. Quintana, Prof. R. Stranger, Prof. M. P. Cifuentes, Prof. M. G. Humphrey
Research School of Chemistry, Australian National University
Canberra, ACT 2601 (Australia)
E-mail: mark.humphrey@anu.edu.au

[**] Part 58: Organometallic Complexes for Nonlinear Optics.

Supporting information and the ORCID identification number(s) for the author(s) of this article can be found under http://dx.doi.org/10.1002/cplu.201600222.

plexes can display significant NLO performance, with the relevant parameters amongst the largest for organometallic complexes.[7] However, the limited examples thus far generally have short π-bridges, and thus the NLO behaviour may not be optimized. We report herein the syntheses of several new azo-containing arylalkyne compounds and derivative alkynyl complexes, spectroscopic and in some cases X-ray structural characterization of the new compounds, spectroscopic, electrochemical, linear and nonlinear optical, and in most cases X-ray structural characterization of the new complexes, comparison to precedents with shorter π-bridges or a related ene/yne-linked composition, and theoretical studies to rationalize the experimental observations.

Results and Discussion

Synthesis and characterization

A specific complex composition was targeted in the present studies. Previous reports had revealed an increase in the key NLO coefficients upon increasing the formal metal valence electron (VE) count,[8] so 18 VE complexes were targeted in the present work. The earlier studies had also shown the efficiency series iron ≤ ruthenium ≤ osmium for Group 8 metal alkynyl complexes,[9] with the facile synthesis of the ruthenium examples more than compensating for their slightly decreased NLO efficiency compared to the kinetically more inert osmium analogues, so the present studies focused on ruthenium complexes. The precedent research had also revealed that pseudo-octahedral complexes *trans*-[Ru(C≡CR)Cl(L_2)$_2$] [L_2 = dppm, dppe; dppm = bis(diphenylphosphino)methane, dppe = 1,2-bis-(diphenylphosphino)ethane] can be highly NLO-efficient and can undergo fully reversible formally $Ru^{II/III}$ redox processes accompanied by strong linear and nonlinear optical changes.[10] Complexes with this specific composition were therefore targeted in the present study.

The alkynyl complexes were accessible in a straightforward way employing existing methodology, namely reaction of the corresponding terminal alkyne with a metal chloride complex.[11] The syntheses of the alkynes proceeded smoothly (Scheme 1), the products being characterized where possible using IR and multinuclear NMR spectroscopies, high-resolution mass spectrometry, and elemental analyses (see the Supporting Information). Thus, reaction of 1-(4-bromophenyl)-2-{4-[(triisopropylsilyl)ethynyl]phenyl}diazene[12] with trimethylsilylacetylene under Sonogashira[13] coupling conditions afforded the difunctionalized trimethylsilylethynyl triisopropylsilylethynyl compound **1** (95%), which was selectively desilylated at the trimethylsilyl group using potassium carbonate to give **2** in excellent yield (93%). A second coupling reaction using 1-iodo-4-nitrobenzene[14] afforded **3** (71%), with azo and yne linkages separating the silyl-protecting group from the nitro acceptor.

Synthesis of the analogue in which the yne linkage is replaced by an *E*-ene group was also successful, albeit in lower overall yield. Oxidation of 4-aminobenzonitrile using potassium peroxymonosulfate[15] afforded the corresponding labile nitrosoarene, which was employed without further purification; reaction with 4-[(triisopropylsilyl)ethynyl]aniline[16] gave the nitrile (*E*)-4-((4-((triisopropylsilyl)ethynylphenyl)diazenyl)benzonitrile (**4**, 75%). Reduction of **4** using (diisobutyl)aluminium hydride (DIBAL-H) afforded the aldehyde **5** (47%) which was reacted with diethyl (4-nitrobenzyl)phosphonate[17] under basic condi-

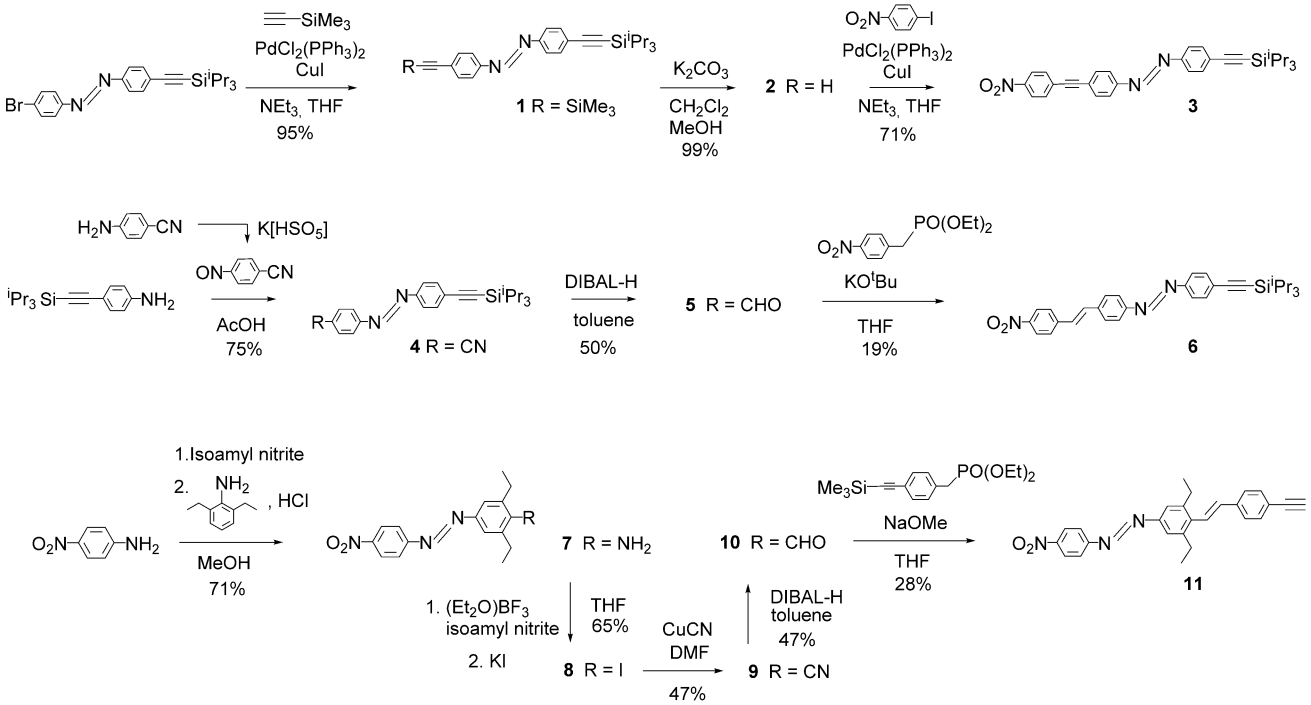

Scheme 1. Preparation of diazene-containing alkynes **3**, **6** and **11**.

tions to afford the silyl-protected terminal acetylene (*E*)-1-[4-((*E*)-4-nitrostyryl)phenyl]-2-{4-[(triisopropylsilyl)ethynyl]phenyl}-diazene (**6**, 19%) in low yield.

The preparation of (*E*)-1-[3,5-diethyl-4-((*E*)-4-ethynylstyryl)-phenyl]-2-(4-nitrophenyl)diazene (**11**), in which the bridging azo and *E*-ene groups of **6** are interchanged, required a sequence including modified Sandmeyer reactions; in contrast to **6**, compound **11** necessitated incorporation of alkyl groups to ensure sufficient solubility. Diazotization of *p*-nitroaniline using isoamyl nitrite as the source of the nitronium ion[18] followed by reaction with 2,6-diethylaniline afforded the diazene (*E*)-2,6-diethyl-4-[(4-nitrophenyl)diazenyl]aniline (**7**, 71%) in good yield. The arylamino group underwent reaction with isoamyl nitrite and then potassium iodide to give the iodo analogue, (*E*)-1-(3,5-diethyl-4-iodophenyl)-2-(4-nitrophenyl)diazene (**8**, 65%), which was in turn reacted with copper(I) cyanide/ferric chloride to give the nitrile (*E*)-2,6-diethyl-4-[(4-nitrophenyl)diazenyl]benzonitrile (**9**) in 47% yield. Reduction of **9** with DIBAL-H afforded the corresponding aldehyde (**10**, 47%) which was reacted with diethyl {4-[(trimethylsilyl)ethynyl]benzyl}phosphonate to give the desired terminal acetylene (**11**, 28%).

The preparation of the new ruthenium complexes proceeded by established methodologies (Scheme 2). Reaction between *cis*-$[RuCl_2(dppm)_2]$[19] and the triisopropylsilyl-protected acetylene **3** in the presence of fluoride afforded **Ru1** (59%); the fluoride desilylated the acetylene in situ, eliminating the need for a further step to isolate the terminal alkyne. The 16-electron, five-coordinate species $[RuCl(dppe)_2]PF_6$[20] was the precursor for the three dppe-containing complexes. It reacted under similar in situ desilylation conditions with the triisopropylsilyl-protected acetylenes **3** and **6** to give **Ru2** (44%) and **Ru3** (55%), respectively, and reacted with the terminal acetylene **11** in the absence of fluoride to give **Ru4** (88%). The vibrational spectra of the complexes possess bands corresponding to the stretching mode of the metal-bound C≡C at 2037–2055 cm^{-1} for **Ru1**–**Ru4**; this band moves to higher energy on replacing dppe by dppm (proceeding from **Ru2** to **Ru1**), replacing an *E*-ene by an yne linkage (proceeding from **Ru3** to **Ru2**) and locating the azo group closer to the nitro (proceeding from **Ru3** to **Ru4**). The $\nu(NO_2)$ vibration is relatively invariant at around 1580 cm^{-1}. The ^{31}P NMR spectra confirm *trans* stereochemistry at the metal center, with a singlet at about −7 ppm for the dppm-containing complex **Ru1**, and at about 49 ppm for the dppe-containing **Ru2**–**Ru4**.

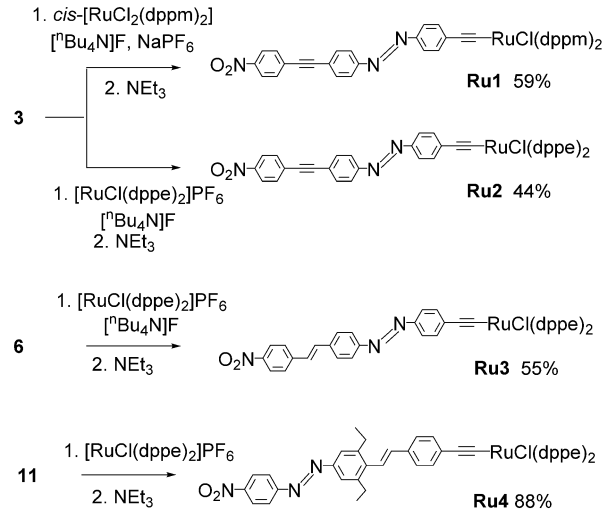

Scheme 2. Syntheses of ruthenium complexes **Ru1**–**Ru4**.

The identities of **3**, **4**, **6**, **8**, **Ru1**, **Ru2**, and **Ru3** were confirmed by single-crystal X-ray diffraction studies (Figure 1 and Figures S1–S7, Tables S1–S3). The bond lengths and angles are unremarkable for the organic compounds and the alkynyl complexes (distortions from colinearity at the Cl1-Ru1-C1-C2-C3 vector are often seen with alkynyl complexes and commonly attributed to packing forces), while the dihedral angles are consistent with good coplanarity through the π-bridges in all complexes.

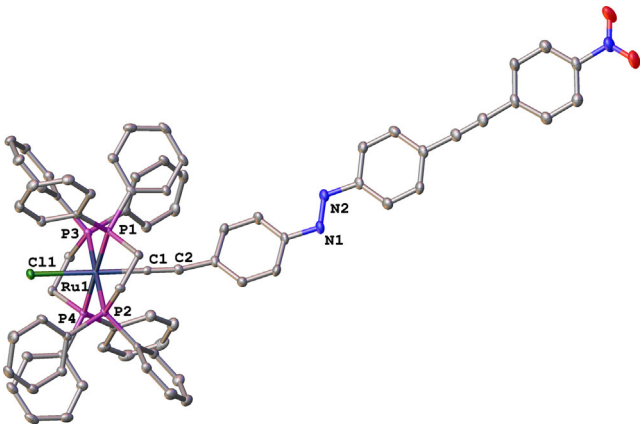

Figure 1. Molecular structure of **Ru2**·CH_2Cl_2, with thermal ellipsoids set at the 40% probability level. Hydrogen atoms and the lattice dichloromethane molecule have been omitted for clarity. Selected bond lengths [Å] and angles [°] are provided in Table S2.

Optical and electrochemical studies

The UV/Vis spectra of the silyl-protected and terminal acetylenes **3**, **6** and **11** show absorption maxima at about 380–400 nm, with the longest-wavelength band due to **6** (Table S5, Figure S8). It is possible that the low-energy bands for **3** and **6** correspond to the superposition of two low-energy bands: the lowest-energy band in the UV/Vis spectrum of **11** is only about half as intense as the low-energy bands of **3** and **6**, and the spectrum of **11** contains a further similar-intensity band at about 289 nm, suggesting that location of the azo group remote from the nitro group (**3**, **6**) red-shifts this band, resulting in its superposition with the existing lowest-energy band.

Coordination of **3** to the ruthenium centre results in a significant bathochromic shift of λ_{max} from 380 nm to 540 nm for the dppm-coordinated complex **Ru1**, and to about 550 nm for the dppe-containing complex **Ru2**. A similar red-shift (from 375 nm to 550 nm) was seen on coupling **11** to the bis(dppe)ruthenium centre in **Ru3** (Figure S9). All of these complexes contain

the diazene group proximal to the metal atom. A slightly smaller shift to 503 nm is seen on coordination of **11** to give **Ru4**, where the diazene group is distal to the ruthenium. Extinction coefficients are similar for **Ru1**–**Ru3**, and slightly lower for **Ru4** (Table 1, Figure S9); this difference in the absorption band intensity is consistent with observations with the precursor alkynes but, in contrast to the alkynes, no clear additional band is apparent at higher energy (although the broad absorption profile makes such analysis difficult). Comparison of the λ_{max} values to that of *trans*-[Ru(C≡C-1-C_6H_4-4-C≡C-1-C_6H_4-4-N=N-1-C_6H_4-4-NO_2)Cl(dppm)$_2$][7a] (**Ru5**, Table 2) confirms the red-shift in proceeding from complexes with a distal diazene to complexes with a proximal electron-withdrawing diazene group.

Table 1. Cyclic voltammetric[a] and UV/Vis[b] data for resting-state and oxidized complexes (measured in CH_2Cl_2).

	$E^{1/2}$ [V] (ΔE [V], i_{pc}/i_{pa})	Ru^{II} $\tilde{\nu}_{max}$ [cm^{-1}] (ε)[c]	Ru^{III} $\tilde{\nu}_{max}$ [cm^{-1}] (ε)[c]
Ru1	0.57 (0.09, 1)	18300 (2.6), 27300 (2.5), 37400 (3.4)	11500 (0.43), 20300 (sh, 1.5), 25200 sh (2.2), 27000 (2.3)
Ru2	0.62 (0.09, 1)	18200 (4.0), 27100 (4.2), 40100 sh (5.8)	11100 (2.6), 21100 (3.6), 38200 (6.1)
Ru3	0.66 (0.05, 1)	18200 (3.8), 26000 (3.8), 40300 (5.2)	11000 (0.68), 20900 (4.2), 38700 (5.7)
Ru4	0.53 (0.09, 1)	19800 (1.1), 26000 (4.7), 40 000 (5.5)	10900 (1.8), 20500 (2.1), 23500 sh (2.5), 26000 (3.0), 36900 (5.7)
Ru6[c]	0.49 (–, 1)	21500 (1.5)	9700 (0.18), 10800 (0.16)

[a] Pt disc working electrode, Pt-wire auxiliary electrode and Ag/AgCl reference electrode, with ferrocene internal standard ($E^{1/2}$ = 0.56 V; [0.09, 1]. [b] cm^{-1}; [10^4 cm^{-1} M^{-1}]. [c] Ref. [11b].

Table 2. Summary of HRS results,[a] and including simple and modified two-level calculations.

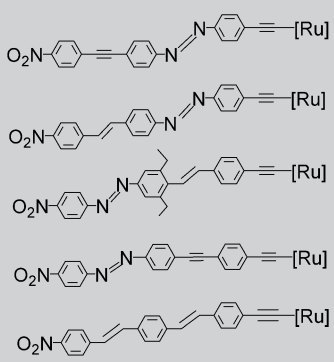

Ru1 [Ru] = *trans*-RuCl(dppm)$_2$
Ru2 [Ru] = *trans*-RuCl(dppe)$_2$
Ru3 [Ru] = *trans*-RuCl(dppe)$_2$
Ru4 [Ru] = *trans*-RuCl(dppe)$_2$
Ru5 [Ru] = *trans*-RuCl(dppm)2
Ru6 [Ru] = *trans*-RuCl(dppm)$_2$
Ru7 [Ru] = *trans*-RuCl(dppe)$_2$

Cmpd	λ_{max}[b]	β_{1064}[c]	β_0[c] $\Delta = 0$	β_0[c] $\Delta = 30$ nm	β_0[c] $\Delta = 50$ nm
Ru1	551	2150	−115	145	185
Ru2	552	2700	−155	190	240
Ru3	548	3200	−140	195	260
Ru4	503	1300	110	125	145
Ru5[d]	510	1215 ± 146	51 ± 6	–	–
Ru6[e]	466	2090 ± 66	395 ± 12	–	–
Ru7[e]	468	2525 ± 175	460 ± 32	–	–

[a] Measured at 1064 nm. [b] nm, **Ru1**–**Ru4**, **Ru6** in CH_2Cl_2, **Ru5**, **Ru7** in THF. [c] 10^{-30} esu in THF. [d] Ref. [7a]. [e] Ref. [11b].

Cyclic voltammetry (CV) studies of solutions of the metal-containing complexes in dichloromethane show a fully reversible $Ru^{II/III}$ oxidation process at 0.62 V (cf. FcH/FcH^+ couple at 0.56 V) (Table 1, Figure S10) for **Ru2**, with a significant shift to a higher potential on replacing the yne linkage with the *E*-ene linkage proceeding to **Ru3** (we recognize that the relevant HOMOs in such ruthenium alkynyl complexes have an alkynyl ligand component, but they certainly have significant metal-centred content, and the redox processes have been labelled as such for simplicity). Changing the coordinated diphosphine ligand from dppe (**Ru2**) to dppm (**Ru1**) results in a slight shift to lower potentials. Oxidation of the metal centre is most easily achieved for **Ru4** (0.53 V), for which the electron-depleting effect of the azo group is reduced due to its increasing distance from the metal. The reduction processes are nitro-centred, occurring at about −0.9 V for **Ru1**–**Ru3**, and −0.8 V for **Ru4**, again consistent with the varying location of the azo group (the electron-withdrawing azo proximal to the nitrophenyl group in **4** results in more facile reduction).

Spectroelectrochemistry allows the measurement of spectral data, in this case UV/Vis-NIR data, whilst a redox potential is applied to a solution of the complex in an optically transparent thin-layer electrochemical (OTTLE) cell. Using the redox data obtained from the CV experiments, oxidation potentials slightly higher than indicated on the CV scans were applied to dichloromethane solutions of **Ru1**–**Ru4**, affording spectral progressions indicating the clean formation of the Ru^{III} species (Figure 2 and Figures S11–S14); subsequent application of a reducing potential to the oxidized species resulted in a return to the starting spectra, with isosbestic points in each case. Frequency maxima and extinction coefficients are collected in Table 1 and show the emergence of a new low-energy band at

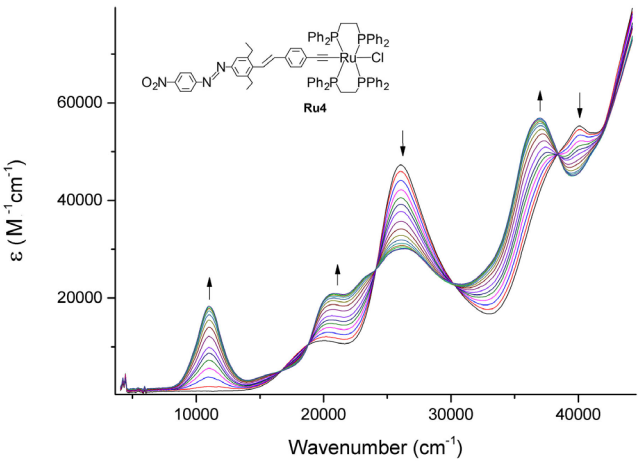

Figure 2. Progressive changes to the UV/Vis-NIR spectra on application of an oxidizing potential of 0.7 V to a solution of **Ru4**. Measured in CH_2Cl_2 at −25 °C. Pt gauze working electrod, Ag wire reference electrode and Pt wire auxillary electrode.

about 11000 cm^{-1} for **Ru1**–**Ru4**, with a progression to lower frequency on replacement of coligand dppm by dppe (proceeding from **Ru1** to **Ru2**), replacement of the yne linkage with the *E*-ene linkage (proceeding from **Ru2** to **Ru3**), or location of the azo group further from the metal centre (proceeding from **Ru2** to **Ru4**).

Hyper-Rayleigh scattering studies

The quadratic nonlinearities of **Ru1**, **Ru2**, **Ru3**, and **Ru4** were determined at 1064 nm using the hyper-Rayleigh scattering (HRS) technique and 20 ns pulses; the results are given in Table 2, together with the two-level-corrected values, and data for related complexes collected under similar conditions. Problems with the two-level model have been discussed previously.[10a] While it is not generally considered adequate for donor–bridge–acceptor organometallics such as those herein, it may be useful in comparing closely related complexes and, with this caveat in mind, one can compare the data. Both experimental and two-level-corrected nonlinearities are consistent with replacement of coligand dppm by dppe leading to an increase in quadratic nonlinearity (proceeding from **1** to **2**). Replacement of the yne linkage by the *E*-ene linkage (proceeding from **2** to **3**) affords data that are within the ±10% error margins. Location of the azo group distal rather than proximal to the metal (proceeding from **Ru2** to **Ru4** or from **Ru1** to **Ru5**) leads to a decrease in quadratic NLO parameters. Further comparison to our previously reported data for **Ru6** and **Ru7** reveals that the frequency-dependent β values for the azo-containing complexes from the present study are comparatively large, but the proximity of the linear optical absorption bands to the second-harmonic wavelength of the Nd:YAG laser employed in the present studies (532 nm) inevitably results in frequency-independent data for the azo-containing compounds that are significantly smaller than those of the *E*-ene-containing analogues.

Various modified two-level models have been proposed to account for the proximity of the second-harmonic wavelength to the optical absorption maximum, and specifically the effects of absorption line broadening and vibrational modes in both the ground and excited states.[21] We have therefore examined our experimental data utilizing the modified two-level model of Wang[21b] [Eq. (1)]:

$$<\beta>_{HRS} = <\beta_0> F(\upsilon,\delta) \quad (1)$$

where $F(\upsilon,\delta) = (1/3)\{[2/(1+2\upsilon)\text{-}1/(1\text{-}\upsilon^2) + 2(1-2\upsilon)/((1-2\upsilon)^2+\delta)]^2 + [2\delta/((1-2\upsilon)^2+\delta^2)]^2\}^{1/2}$, $\upsilon = \lambda_{max}/\lambda$, $\delta = \Delta/\lambda_{max}$, Δ is a damping factor associated with the broadening of the absorption peak, and λ is the fundamental light wavelength (1064 nm in this case). Note that, if $\Delta = 0$, the expression above simplifies to that of the usual two-level model. Using this equation and assuming that Δ is 30–50 nm (estimated from the UV/Vis spectra: Δ likely differs from sample to sample), the recalculated $<\beta_0>$ values are listed in Table 2. For **Ru4**, the recalculated $<\beta_0>$ is close to that calculated with the simple two-level model, while for **Ru1**–**Ru3**, for which λ_{max} values are close to 550 nm, the modified two-level model yields a greater discrepancy; nevertheless, the trend in experimental maximal values (**Ru3** > **Ru2** > **Ru1** > **Ru4**) is maintained for the various two-level approximations.

Computational studies

Time-dependent density functional theory (TD-DFT) calculations were undertaken on a set of model complexes (Figure 3)

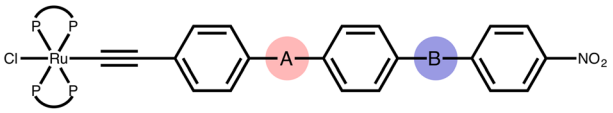

Complex	A	B
Ru2'	(*E*)-N=N-	-C≡C-
Ru3'	(*E*)-N=N-	(*E*)-HC=CH-
Ru4'	(*E*)-HC=CH-	(*E*)-N=N-

Figure 3. Model compounds used in computational studies. P–P = $Me_2PCH_2CH_2PMe_2$.

to rationalize the experimental UV/Vis spectra. Calculated low-lying (< 30000 cm^{-1}) singlet excited-state transitions and oscillator strengths are listed in Table S7, alongside the experimental data. Frontier molecular orbitals (FMOs) involved in the main transitions for the model compounds **Ru2**′ and **Ru4**′ are given in Figures S15 and S16, respectively; the FMOs obtained for **Ru2**′ and **Ru3**′ are very similar in their composition.

Calculated transitions for all model complexes in the lower-energy region (< 30000 cm^{-1}) can be divided into two different groups; each model complex exhibits an intense transition in the region 15000 cm^{-1} to 17000 cm^{-1} and one or two transitions with large oscillator strengths in the region 21500 cm^{-1} to 25000 cm^{-1}. The calculated data are consistent with the experimental data, particularly for model compounds **Ru2**′ and **Ru3**′. The second spectral band for **Ru2** and **Ru3** is broader than the lowest-energy band; this can be attributed to the presence of several transitions close in energy in this region, according to the calculated data (Table S7). The experimental lowest-energy band is slightly more intense than the second lowest-energy band, and this behaviour is nicely reproduced by the computational outcomes of the corresponding model compounds (**Ru2**′/**Ru3**′). In the case of **Ru4**′, these calculated transitions are substantially red-shifted compared to the UV/Vis data. However, the incorporation of ethyl substituents in the laboratory complex **Ru4** to overcome the solubility problems may induce steric crowding around the *E*-ene linkage in the coplanar conformation, and thus distort the complex from the ideal coplanar arrangement of the phenylene groups which is assumed in these calculations. Further calculations reveal that distortion from a coplanar structure blue-shifts the low-lying transitions, in particular the lowest-energy band, and decreases their intensity.

Although the highest occupied molecular orbital (HOMO) for all model compounds is broadly similar (i.e. the HOMO is mainly located on the ClRuC≡C-1-C_6H_4-4- moiety; Figures S15 and S16), the lowest unoccupied molecular orbitals (LUMOs) in **Ru2′** (and **Ru3′**) are delocalized on the N=N-1-C_6H_4-4-C≡C-1-C_6H_4-4-NO_2 group, whereas in **Ru4′** electron density is primarily located at the N=N-1-C_6H_4-4-NO_2 group, particularly at the azophenylene unit. Overall, the lowest-energy LUMO (L)←HOMO (H) transition involves a mixture of metal-to-ligand charge transfer (MLCT) and intraligand CT (ILCT) character, together with some contribution from ligand-to-ligand CT (LLCT).

The second- and third-lowest energy transitions, which lead to a somewhat broad band in the experimental UV/Vis spectrum of **Ru2** (and **Ru3**), originate from L+1←H and L←H−2 electronic transitions. H−2 differs from H in that density leaks into the central part of the bridge [that is, the N=N-1-C_6H_4-4-C≡C unit]. π-bonding within the azo and yne groups (or the *E*-ene group in **Ru3′**) also contributes to H−2. L+1 is primarily N=N (π*) and 1-C_6H_4-4-NO_2 C-N (π) based. The second-lowest-energy transition for the model complex **Ru4′** is characterized as promotion from H−2 (dominated by electron density around the ClRuC≡C-1-C_6H_4-4-C≡C-1-C_6H_4-4 unit) to L.

Static first hyperpolarizability values, β_{tot}, were calculated for all model complexes (Table S8). Replacing an yne linkage with an *E*-ene unit, on proceeding from **Ru2′** to **Ru3′**, has little effect on β_{tot}, an outcome that is consistent with laboratory observations (Table 2 and Table S8). The position of the azo linkage exerts a significant influence on the β value; the calculated findings clearly indicate that the complex in which the *E*-azo linkage is distal from the metal exhibits a much larger nonlinear response than the proximal isomer (proceeding from **Ru3′** to **Ru4′** leads to an approximately twofold increase in calculated β), although this is contrary to experimental observations. Given the discrepancy with experimental data for the latter, the performance of calculations in reproducing these structure–property outcomes was examined as a function of the method used (PBEPBE (the principal method used in these studies), CAM-B3LYP, and LC-PBEPBE: see the Supporting Information); all methods suggest that β increases significantly when the *E*-azo linkage changes its position from A to B (Figure 3), whereas replacing an yne group with an *E*-ene linkage has a minor effect.

The simple two-level model (TLM) developed by Oudar and Chemla[22] is widely used for extrapolating the experimental hyper-Rayleigh scattering (HRS) data (frequency-dependent β value) to the static first hyperpolarizability, but this simple model is not applicable when the scattered photon frequency approaches the resonance frequency of the CT transition[21b,23] (see above), and thus the simple TLM is not suitable for evaluating the static hyperpolarizability of laboratory analogues of model complexes **Ru2′** and **Ru3′** (in particular) as they exhibit transitions very close to the second harmonic at 532 nm. Hence, Equation (3) in the Supporting Information, which extends the simple two-level model into the resonant regime,[21b] was used to calculate the static values. However, Equation (3) assumes that only two electronic states contribute to the first hyperpolarizability, β^{CT}. It should be used with great caution when two spectral bands relatively close in energy exhibit MLCT character; this is particularly the case with **Ru2** and **Ru3**, for which the high-energy bands may also contribute to the overall β. It should also be noted that although we considered only the lowest-energy band when deriving the experimental static value for **Ru4**, a contribution from the more intense second-lowest-energy band (which is predominantly MLCT in character) to the $\beta_{0,exp}$ should also be taken into account.

Ru2′ and **Ru3′** show similar linear optical behaviour in the low-energy region, possessing almost identical lowest-energy transitions. Moreover, the degree of MLCT character of these bands, on the basis of calculations, is almost the same, and thus it is not surprising that replacing an yne linkage with an *E*-ene group on proceeding from **Ru2′** to **Ru3′** has only a minor effect on the β value. In contrast, the calculated UV/Vis spectrum of **Ru4′** contains a significantly red-shifted lowest-energy transition compared to the lowest-energy transitions for **Ru2′** and **Ru3′**, which may account for the large β_{tot} calculated for model compound **Ru4′**.

Conclusion

The new complexes **Ru1**–**Ru4** and the previously reported **Ru5**–**Ru7** afford a suite of complexes that permit comment on the effect of azo group introduction and location on electronic and optical properties of metal alkynyl complexes. The $Ru^{II/III}$ oxidation potentials shift to higher potential on replacing yne linkage with *E*-ene linkage (proceeding from **Ru2** to **Ru3**), changing the coordinated diphosphine ligand from dppm (**Ru1**) to dppe (**Ru2**), and locating the azo group proximal to the metal centre (proceeding from **Ru4** to **Ru1**, **Ru2**, and **Ru3**); the last-mentioned observation is consistent with previous studies of ruthenium alkynyl complexes for which the electron-withdrawing influence of groups is particularly pronounced when they are appended to the proximal (to ruthenium) ring.[10a] The wavelength of the UV/Vis λ_{max} band can be tuned by bridge variation, red-shifting on proceeding from complexes bearing *E*-ene linkages (e.g. *trans*-[Ru(C≡C-1-C_6H_4-4-(*E*)-CH=CH-1-C_6H_4-4-(*E*)-CH=CH-1-C_6H_4-4-NO_2)Cl(dppe)$_2$] (**Ru7**): 468 nm) to the complex with a distal azo group (**Ru4**: 503 nm) to complexes with a proximal azo group (**Ru1**–**Ru3**: 540–550 nm). The frequency-dependent β values for the azo-containing complexes from the present study are comparatively large (ca. 3000×10^{-30} esu for **Ru2** and **Ru3**) but strongly resonance enhanced; experimental values for **Ru2** and **Ru3** are similar to that of **Ru7**, but the two-level-corrected data for the azo-linked compounds are much smaller than that of the ene-linked **Ru7** and, while being mindful of the problems associated with this approximation, we conclude that the ene-linked alkynyl complexes are more efficient NLO materials. The formally Ru^{III} complexes exhibit low-energy bands at about 11 000 cm^{-1} for **Ru1**–**Ru4**, and the location of this LMCT band can be tuned by molecular modification; it moves to lower frequency on replacement of coligand dppm by dppe (proceeding from **Ru1** to **Ru2**), replacement of yne linkage with *E*-ene linkage (proceeding from **Ru2** to **Ru3**), or location of the azo group further from the metal centre (proceeding from **Ru2** to

Ru4). Thus, **Ru1**–**Ru4** are in principle electrochemically—($Ru^{II/III}$) as well as photochemically—(*E*⇔*Z* azo) switchable optical materials.

Computational studies were undertaken on models **Ru2**′–**Ru4**′ to rationalize this optical behaviour. Calculations agree well with the experimental linear optical data, although we found a mismatch between the calculated and experimental lowest-energy bands for **Ru4** as a consequence of employing a fully planar structure for **Ru4**′ to represent the laboratory compound **Ru4**. In **Ru4**′, the ethyl substituents used as an aid to mitigate solubility problems in **Ru4** are removed because they may cause distortions in the bridge, and thus adversely affect both empirical peak position and intensity of the lowest-energy band. On the basis of calculations, the HOMO for all three model systems is broadly similar and mainly located on the ClRuC≡C-1-C_6H_4-4- unit, while the LUMO for **Ru4**′ is more localized compared to that for **Ru2**′ and **Ru3**′. The LUMOs for **Ru2**′ and **Ru3**′ are delocalized on the N=N-1-C_6H_4-4-C≡C-1-C_6H_4-4-NO_2 group, and in **Ru4**′ primarily located at the distal N=N-1-C_6H_4-4-NO_2 group. The lowest-energy bands associated with L←H excitation can be ascribed to a mixture of MLCT and ILCT character with a LLCT contribution. Although the decrease in β value on proceeding from **Ru2**–**Ru3** to **Ru4** is not reproduced computationally, due to a distorted non-coplanar structure for laboratory compound **Ru4**, as discussed earlier, both the experimental and calculated data reveal that replacing an yne linkage with an *E*-ene group on proceeding from **Ru2** to **Ru3** (or **Ru2**′ to **Ru3**′) has only a minor effect on the β value due to the similar linear optical properties they possess in the low-energy region.

Acknowledgements

We thank the Australian Research Council (ARC), the National Natural Science Foundation of China (51432006), and the Chinese Government Ministry of Education and State Administration of Foreign Experts Affairs (111 Project: B13025) for financial support. M.P.C. thanks the ARC for an Australian Research Fellowship.

Keywords: alkene ligands · alkyne ligands · electrochemistry · nonlinear optics · transition metals

[1] a) P. N. Prasad, D. J. Williams, *Introduction to Nonlinear Optical Effects in Molecules and Polymers*, Wiley, New York, **1991**; b) J. Zyss, *Molecular Nonlinear Optics: Materials, Physics and Devices*, Academic Press, Boston, **1994**; c) D. M. Roundhill, J. P. Fackler Jr., *Optoelectronic Properties of Inorganic Compounds*, Plenum, New York, **1999**.

[2] a) V. P. Rao, A. K. Y. Jen, K. Y. Wong, K. J. Drost, *J. Chem. Soc. Chem. Commun.* **1993**, 1118–1120; b) L. Qiu, Y. Shen, J. Hao, J. Zhai, F. Zu, T. Zhang, Y. Zhao, K. Clays, A. Persoons, *J. Mater. Sci.* **2004**, *39*, 2335–2340; c) J.-M. Raimundo, P. Blanchard, N. Gallego-Planas, N. Mercier, I. Ledoux-Rak, R. Hierle, J. Roncali, *J. Org. Chem.* **2002**, *67*, 205–218; d) A. J. Moore, A. Chesney, M. R. Bryce, A. S. Batsanov, J. F. Kelly, J. A. K. Howard, I. F. Perepichka, D. F. Perepichka, G. Meshulam, G. Berkovic, Z. Kotler, R. Mazor, V. Khodorkovsky, *Eur. J. Org. Chem.* **2001**, 2671–2687; e) S. R. Marder, J. W. Perry, B. G. Tiemann, C. B. Gorman, S. Gilmour, S. L. Biddle, G. Bourhill, *J. Am. Chem. Soc.* **1993**, *115*, 2524–2526; f) M. Blanchard-Desce, V. Bloy, J.-M. Lehn, C. Runser, M. Barzoukas, A. Fort, J. Zyss, *Proc. SPIE-Int. Soc. Opt. Eng.* **1994**, *2143*, 20–29; g) C. R. Moylan, R. J. Twieg, V. Y. Lee, S. A. Swanson, K. M. Betterton, R. D. Miller, *J. Am. Chem. Soc.* **1993**, *115*, 12599–12600; h) F. Würthner, F. Effenberger, R. Wortmann, P. Kraemer, *Chem. Phys.* **1993**, *173*, 305–314; i) E. M. Breitung, C.-F. Shu, R. J. McMahon, *J. Am. Chem. Soc.* **2000**, *122*, 1154–1160; j) M. Matsui, M. Suzuki, M. Hayashi, K. Funabiki, Y. Ishigure, Y. Doke, H. Shiozaki, *Bull. Chem. Soc. Jpn.* **2003**, *76*, 606–607; k) M. Barzoukas, M. Blanchard-Desce, D. Josse, J. M. Lehn, J. Zyss, *Chem. Phys.* **1989**, *133*, 323–329; l) B. K. Spraul, S. Suresh, T. Sassa, M. Angeles Herranz, L. Echegoyen, T. Wada, D. Perahia, D. W. Smith, *Tetrahedron Lett.* **2004**, *45*, 3253–3256; m) T.-G. Zhang, M. J. Therien, *Polym. Prepr. Am. Chem. Soc. Div. Polym. Chem.* **2002**, *43*, 570–571; n) R. Twieg, V. Lee, R. D. Miller, C. R. Moylan, *Polym. Prepr. Am. Chem. Soc. Div. Polym. Chem.* **1994**, *35*, 200–201; o) S. Priyadarshy, M. J. Therien, D. N. Beratan, *J. Am. Chem. Soc.* **1996**, *118*, 1504–1510; p) M. Moreno-Mañas, R. Pleixats, R. Andreu, J. Garin, J. Orduna, B. Villacampa, E. Levillain, M. Sallé, *J. Mater. Chem.* **2001**, *11*, 374–380; q) S. R. Marder, B. G. Tiemann, A. Friedli, E. Yang, L.-T. Cheng, *Nonlinear Opt.* **1995**, *9*, 213–221; r) A. K. Y. Jen, T.-A. Chen, V. P. Rao, Y. Cai, Y.-J. Liu, L. R. Dalton, *Adv. Nonlinear Opt.* **1997**, *4*, 237–249; s) M. Barzoukas, A. Fort, G. Klein, C. Serbutoviez, L. Oswald, J. F. Nicoud, *Chem. Phys.* **1992**, *164*, 395–406.

[3] T. Tsunekawa, K. Yamaguchi, *J. Phys. Chem.* **1992**, *96*, 10268.

[4] V. Guerchais, H. Bozec, *Molecular Organometallic Materials for Optics in Top. Organomet. Chem., Vol. 28*, Springer, Berlin, Heidelberg, **2010**, pp. 171–225.

[5] a) J. P. L. Morrall, G. T. Dalton, M. G. Humphrey, M. Samoc, *Adv. Organomet. Chem.* **2007**, *55*, 61–136; b) M. G. Humphrey, T. Schwich, P. J. West, M. P. Cifuentes, M. Samoc in *Comprehensive Inorganic Chemistry II, Vol. 8* (Eds.: J. Reedijk, K. Poeppelmeier), Elsevier, Oxford, **2013**, pp. 781–835.

[6] a) B. J. Coe, S. Houbrechts, I. Asselberghs, A. Persoons, *Angew. Chem. Int. Ed.* **1999**, *38*, 366–369; *Angew. Chem.* **1999**, *111*, 377–380; b) B. J. Coe, N. R. M. Curati, *Comments Inorg. Chem.* **2004**, *25*, 147–184; c) I. Asselberghs, K. Clays, A. Persoons, A. M. McDonagh, M. D. Ward, J. McCleverty, *Chem. Phys. Lett.* **2003**, *368*, 408–411.

[7] a) T. N. Fondum, K. A. Green, M. D. Randles, M. P. Cifuentes, A. C. Willis, A. Teshome, I. Asselberghs, K. Clays, M. G. Humphrey, *J. Organomet. Chem.* **2008**, *693*, 1605–1613; b) A. M. McDonagh, N. T. Lucas, M. P. Cifuentes, M. G. Humphrey, S. Houbrechts, A. Persoons, *J. Organomet. Chem.* **2000**, *605*, 184–192.

[8] a) I. R. Whittall, M. P. Cifuentes, M. G. Humphrey, B. Luther-Davies, M. Samoc, S. Houbrechts, A. Persoons, G. A. Heath, D. Bogsanyi, *Organometallics* **1997**, *16*, 2631–2637; b) I. R. Whittall, M. G. Humphrey, S. Houbrechts, A. Persoons, D. C. R. Hockless, *Organometallics* **1996**, *15*, 5738–5745.

[9] C. E. Powell, M. P. Cifuentes, A. M. McDonagh, S. Hurst, N. T. Lucas, C. D. Delfs, R. Stranger, M. G. Humphrey, S. Houbrechts, I. Asselberghs, A. Persoons, D. C. R. Hockless, *Inorg. Chim. Acta* **2003**, *352*, 9–18.

[10] a) S. Hurst, M. P. Cifuentes, J. P. L. Morrall, N. T. Lucas, I. R. Whittall, M. G. Humphrey, I. Asselberghs, A. Persoons, M. Samoc, B. Luther-Davies, A. C. Willis, *Organometallics* **2001**, *20*, 4664–4675; b) R. H. Naulty, A. M. McDonagh, I. R. Whittall, M. P. Cifuentes, M. G. Humphrey, S. Houbrechts, J. Maes, A. Persoons, G. A. Heath, D. C. R. Hockless, *J. Organomet. Chem.* **1998**, *563*, 137–146; c) R. H. Naulty, M. P. Cifuentes, M. G. Humphrey, S. Houbrechts, C. Boutton, A. Persoons, G. A. Heath, D. C. R. Hockless, B. Luther-Davies, M. Samoc, *J. Chem. Soc. Dalton Trans.* **1997**, 4167–4175.

[11] a) D. Touchard, P. Haquette, N. Pirio, L. Toupet, P. H. Dixneuf, *Organometallics* **1993**, *12*, 3132–3139; b) L. Rigamonti, B. Babgi, M. P. Cifuentes, R. L. Roberts, S. Petrie, R. Stranger, S. Righetto, A. Teshome, I. Asselberghs, K. Clays, M. G. Humphrey, *Inorg. Chem.* **2009**, *48*, 3562–3572.

[12] T.-T.-T. Nguyen, D. Türp, D. Wang, B. Nölscher, F. Laquai, K. Müllen, *J. Am. Chem. Soc.* **2011**, *133*, 11194–11202.

[13] K. Sonogashira, Y. Tohda, N. Hagihara, *Tetrahedron Lett.* **1975**, *16*, 4467–4470.

[14] A. Yassin, P. Jimenez, B. Lestriez, P. Moreau, P. Leriche, J. Roncali, P. Blanchard, H. Terrisse, D. Guyomard, J. Gaubicher, *Chem. Mater.* **2015**, *27*, 4057–4065.

[15] A. Zarei, A. R. Hajipour, L. Khazdooz, *Synthesis* **2009**, 941–944.

[16] S. Zarwell, K. Rueck-Braun, *Tetrahedron Lett.* **2008**, *49*, 4020–4025.

[17] N. G. Anthony, D. Breen, J. Clarke, G. Donoghue, A. J. Drummond, E. M. Ellis, C. G. Gemmell, J.-J. Helesbeux, I. S. Hunter, A. I. Khalaf, S. P. Mackay,

J. A. Parkinson, C. J. Suckling, R. D. Waigh, *J. Med. Chem.* **2007**, *50*, 6116 – 6125.
[18] T. Fehrentz, C. A. Kuttruff, F. M. E. Huber, M. A. Kienzler, P. Mayer, D. Trauner, *ChemBioChem* **2012**, *13*, 1746 – 1749.
[19] B. Chaudret, G. Commenges, R. Poilblanc, *J. Chem. Soc. Dalton Trans.* **1984**, 1635 – 1639.
[20] H. Zhao, P. V. Simpson, A. Barlow, G. J. Moxey, M. Morshedi, N. Roy, R. Philip, C. Zhang, M. P. Cifuentes, M. G. Humphrey, *Chem. Eur. J.* **2015**, *21*, 11843 – 11854.
[21] a) A. M. Kelley, *J. Opt. Soc. Am. B* **2002**, *19*, 1890 – 1900; b) C. H. Wang, *J. Chem. Phys.* **2000**, *112*, 1917 – 1924.
[22] J. L. Oudar, D. S. Chemla, *J. Chem. Phys.* **1977**, *66*, 2664 – 2668.
[23] a) M. P. Robalo, A. P. S. Teixeira, M. H. Garcia, M. F. Minas da Piedade, M. T. Duarte, A. R. Dias, J. Campo, W. Wenseleers, E. Goovaerts, *Eur. J. Inorg. Chem.* **2006**, 2175 – 2185; b) I. R. Whittall, M. P. Cifuentes, M. G. Humphrey, B. Luther-Davies, M. Samoc, S. Houbrechts, A. Persoons, G. A. Heath, D. C. R. Hockless, *J. Organomet. Chem.* **1997**, *549*, 127 – 137.

Manuscript received: April 27, 2016
Accepted Article published: May 23, 2016
Final Article published: ■■ ▮▮, 0000

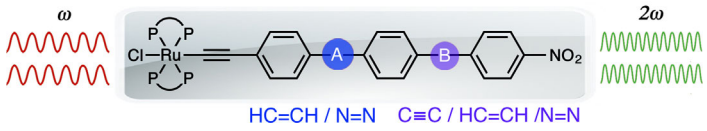

It takes alkynes: Dipolar organometallic complexes with a ligated ruthenium donor, nitro acceptor, and a π-delocalizable bridge incorporating an azo group exhibit large quadratic optical nonlinearities (see figure). The potentials of their reversible oxidation processes and the wavelengths of their absorption maxima in both the resting and oxidized forms are tuned by systematic structural modification.

*D. Wei, M. S. Kodikara, M. Morshedi, G. J. Moxey, H. Wang, G. Wang, C. Quintana, C. Zhang, R. Stranger, M. P. Cifuentes, M. G. Humphrey**

■■ – ■■

Syntheses and Optical Properties of Azo-Functionalized Ruthenium Alkynyl Complexes